Tunable Supermode Dielectric Resonators for Axion Dark-Matter Haloscopes

Ben T. McAllister,[1,*] Graeme Flower,[1] Lucas E. Tobar,[1,2] and Michael E. Tobar[1,†]
[1]ARC Centre of Excellence for Engineered Quantum Systems, School of Physics, The University of Western Australia, Crawley 6009, Australia
[2]Department of Electrical and Computer Systems Engineering, Monash University, Clayton 3800, Australia

(Received 16 June 2017; revised manuscript received 19 September 2017; published 26 January 2018)

We present frequency-tuning mechanisms for dielectric resonators, which undergo "supermode" interactions as they tune. The tunable schemes are based on dielectric materials strategically placed inside traditional cylindrical resonant cavities, necessarily operating in transverse-magnetic modes for use in axion haloscopes. The first technique is based on multiple dielectric disks with radii smaller than that of the cavity. The second scheme relies on hollow dielectric cylinders similar to a Bragg resonator, but with a different location and dimension. Specifically, we engineer a significant increase in form factor for the TM_{030} mode utilizing a variation of a distributed Bragg reflector resonator. Additionally, we demonstrate an application of traditional distributed Bragg reflectors in TM modes which may be applied to a haloscope. Theoretical and experimental results are presented showing an increase in Q factor and tunability due to the supermode effect. The TM_{030} ring-resonator mode offers a between 1 and 2-order-of-magnitude improvement in axion sensitivity over current conventional cavity systems and will be employed in the forthcoming ORGAN experiment.

DOI: 10.1103/PhysRevApplied.9.014028

I. INTRODUCTION

For many years, scientists have suspected the presence of a large amount of so called "dark matter" in the galactic halo, motivated by a number of gravitational observations. However, the nature of this matter remains unknown, although many have suggested that it may be composed of new particles not included in the standard model. One popular dark-matter candidate is a weakly interacting slim particle [1] known as the axion. Axions were first proposed in 1977 as a consequence of an elegant solution to the strong CP problem in QCD [2]. Since the expected properties of the axion (finite mass with weak coupling to regular matter) align with the desired properties of dark matter, it was proposed in 1983 that dark matter might be composed of axions [3].

The most mature and common laboratory search technique for axions is known as the haloscope, which was first proposed by Sikivie in 1983 [4,5]. The haloscope aims to detect axions via their coupling to photons. It is thought that axions will convert into photons in the presence of other photons (a form of the Primakoff effect). In most haloscopes, a strong, external static magnetic field provides a source of virtual photons for axions to scatter off and create real photons. Because of conservation of energy, the frequency of the generated real photon corresponds directly to the mass of the axion (with some narrow linewidth as a result of velocity dispersion). Many axion haloscopes are currently operational, most notably the Axion Dark Matter Experiment, the first and most mature such experiment [6,7].

A confounding concern for axion haloscopes is the fact that the mass of the axion is largely unknown (other than some broad cosmological limits [8,9]), meaning that the frequency of the generated photons is also unknown. Additionally, the strength of the axion coupling to photons is unknown, which creates a large parameter space for searching. The critical parameter which haloscopes ultimately wish to constrain or bound is the Peccei-Quinn symmetry breaking scale, f_a. This scale determines both the axion mass and the strength of its coupling to photons according to

$$m_a \sim \frac{4.51 \times 10^{15}}{f_a}\ \text{eV}$$
$$g_{a\gamma\gamma} = \frac{g_\gamma \alpha}{f_a \pi}.$$

Here, g_γ is an axion-model-dependent parameter of order 1, and α is the fine-structure constant [10–14].

II. HALOSCOPES AND DIELECTRIC MATERIALS

In a haloscope, a resonant cavity is embedded in a strong static magnetic field. If axions are present due to an abundance in galactic-halo dark matter, a small number will convert into real photons with a frequency corresponding to the axion mass. It is advantageous to tune the

*ben.mcallister@uwa.edu.au
†michael.tobar@uwa.edu.au

resonant frequency of the cavity to the corresponding photon frequency in order for the signal to be resonantly enhanced. Once the signal is trapped in the cavity, it can be read out via low-noise electronics. The expected signal power in a haloscope is given by [15]

$$P_a \propto g_{a\gamma\gamma}^2 B^2 C V Q_L \frac{\rho_a}{m_a}.$$

Here, B is the field strength of the external magnetic field, V is the volume of the detecting cavity, Q_L is the loaded-cavity quality factor (provided it is lower than the expected axion-signal quality factor of approximately 10^6), ρ_a is the local axion dark-matter density, and C is a mode-dependent form factor of order 1 [16], defined generally in dielectric and magnetic materials as

$$C = \frac{|\int dV_c \vec{E_c} \cdot \vec{\hat{z}}|^2}{2V \int dV_c \epsilon_r |E_c|^2} + \frac{\frac{\omega_a^2}{c^2} |\int dV_c \frac{r}{2} \vec{B_c} \cdot \vec{\hat{\phi}}|^2}{2V \int dV_c \frac{1}{\mu_r} |B_c|^2}.$$

Here, E_c and B_c are the cavity electric and magnetic fields, respectively, and ϵ_r and μ_r are the relative dielectric and magnetic constants of the media. It is worth noting that the two terms in this equation are equal to one another, and we may present it as

$$C = \frac{|\int dV_c \vec{E_c} \cdot \vec{\hat{z}}|^2}{V \int dV_c \epsilon_r |E_c|^2}. \tag{1}$$

We could equivalently present the shorter equation as twice the second term in the full equation, depending on B_ϕ. The scanning rate of a haloscope is given by [17]

$$\frac{df}{dt} \propto \frac{1}{\mathrm{SNR}_{\mathrm{goal}}^2} \frac{g_{a\gamma\gamma}^4 B^4 C^2 V^2 \rho_a^2 Q_L Q_a}{m_a^2 (k_B T_n)^2}. \tag{2}$$

Here $\mathrm{SNR}_{\mathrm{goal}}$ is the desired signal-to-noise ratio of the search, Q_a is the axion-signal quality factor, and T_n is the effective noise temperature of the first stage amplifier, with later amplifier contributions suppressed by the gain of this amplifier. This is the quantity that must be maximized in design of an experiment, for which $C^2 V^2 G$ can be viewed as a figure of merit for resonator design, as these are the only resonator-dependent terms. G is the mode geometry factor given by

$$G = \frac{\omega \mu_0 \int |\vec{H}|^2 dV}{\int |\vec{H}|^2 dS},$$

which is directly proportional to the mode quality factor according to

$$Q = \frac{G}{R_s},$$

where ω is the angular resonant frequency, μ_0 is the permeability of free space, $\vec{H}$ is the cavity magnetic field, and R_s is the surface resistance of the material. In this calculation, there is the implicit assumption that any dielectric adds no loss. This assumption is valid when using low-loss materials such as sapphire and rutile [18–20], as the loss produced at the cavity walls will usually be orders of magnitude greater for transverse-magnetic (TM) modes with an azimuthal mode number of zero. Otherwise, one must compute the filling factor in the dielectric and multiply by its loss tangent to calculate the effect on the Q factor.

Recently, there has been much interest in the use of dielectric materials in axion haloscopes [21–23]. There are many reasons for this interest. First, as evident in the form-factor expression given by Eq. (1), the relative dielectric constant of a medium has an impact on the coupling of the axion to the cavity resonance, and this dependence can be exploited to boost the form factor with careful placement of the dielectrics. Second, dielectric resonators are well known for their high quality factors and are often employed in other areas, such as metrology, where high-quality resonances are required. Additionally, the introduction of dielectrics into a cavity provides many more free parameters and opportunities for broken symmetry that can be exploited to create a frequency-tuning mechanism.

Furthermore, as there is increased interest in axion searches in mass ranges above and below the range traditionally searched by cavity experiments [24–30], dielectrics have attracted increased interest due to their ability to lower the resonant frequency of a cavity by lowering the speed of propagation of resonant photons, or increasing the effective optical-path length.

In the push towards higher frequency and mass searches, it would be beneficial to utilize high-order resonant modes, as they can provide high-frequency resonances in large resonator volumes. However, in a traditional empty resonator, higher-order resonances have significantly reduced form factors due to a high degree of field variation. For example, comparing a TM_{010} mode with a TM_{020} mode in the empty cavity, the lower-order mode has all of its E_z field in the same direction, and thus the form factor is high (approximately 0.69). By contrast, the higher-order mode has an out-of-phase E_z field component which "cancels out" part of the coupling and reduces the form factor to about 0.13. As we discuss below, careful placement of dielectric materials can assist with this problem. Moreover, the modes in the empty cavity resonator have frequencies which are independent of length, and elaborate tuning mechanisms must therefore be implemented [17]. We show in the proceeding section that the concept of supermode tuning allows for altering resonator frequency by simply varying the positions of two components of the resonator along the length of the cylinder.

III. DIELECTRIC-RESONATOR PROPOSALS

The Electric Tiger and MADMAX experiments propose utilizing multiple dielectric disks or slabs and simultaneously tuning multiple gap spacings [21,31,32], with the former being a resonant system and the latter broadband. While sensitive and valuable proposals, they present some practical challenges. One potential problem with such modes in a resonant system is that they are of extremely high order and, without proper design, can suffer from mode crowding and require the disks to be larger than the spot size to maintain a high Q factor. In this work, we propose a different technique which utilizes a supermode tuning mechanism in a dielectric loaded-cavity resonator. For this technique, only two pieces of dielectric are required (utilizing more pieces is possible but does not offer any advantages) and, like MADMAX and Electric Tiger, the tuning is "built-in," which is to say that we do not need to introduce extra material into the cavity to tune the modes. We propose two different types of dielectric resonators which utilize this technique, and we determine the sensitivity of each scheme to axions. We compare these results with a haloscope tuned by traditional means.

A. Dielectric disks

The first scheme proposed here relies on multiple dielectric disks (with a minimum of 2), located in a cylindrical conducting shell with a variable gap between them. The simplest dielectric modes that tune in frequency are known as supermodes [33–35]. In the two-disk structure, symmetric and antisymmetric supermodes span both cylindrical disks of the dielectric (in this case, sapphire) and occupy the entire volume. The magnetic field B_ϕ density plots are shown in Fig. 1, computed using the finite-element method in COMSOL MULTIPHYSICS. The higher-frequency mode is the antisymmetric mode with a zero in the field between the two disks and each antinode out of phase, while the symmetric mode is lower in frequency, with two antinodes in phase. In the limit where the gap spacing is large, the frequency of the symmetric mode approaches the frequency of the antisymmetric mode with the final mode separation depending on the mode confinement within the dielectric. This effect can be seen in Fig. 2. The initial frequency difference between the symmetric and antisymmetric modes defines the potential maximum possible tuning range using this technique. We note that these symmetric and antisymmetric supermodes arise as perturbed versions of the cavity TM_{012} and TM_{013} modes, respectively. The analytical solutions for the B_ϕ components of TM_{01p} modes are

$$B_\phi(r,z) \propto J_0'\left(\frac{\zeta_{0,1}}{R}r\right)\cos\left(\frac{p\pi}{L}z\right), \tag{3}$$

where J_0' is the derivative of the zeroth-order Bessel J function, $\zeta_{0,1}$ is the first root of the zeroth-order Bessel J function, R is the cavity radius, and L is the cavity length. If we observe the B_ϕ mode profiles as a function of z for a

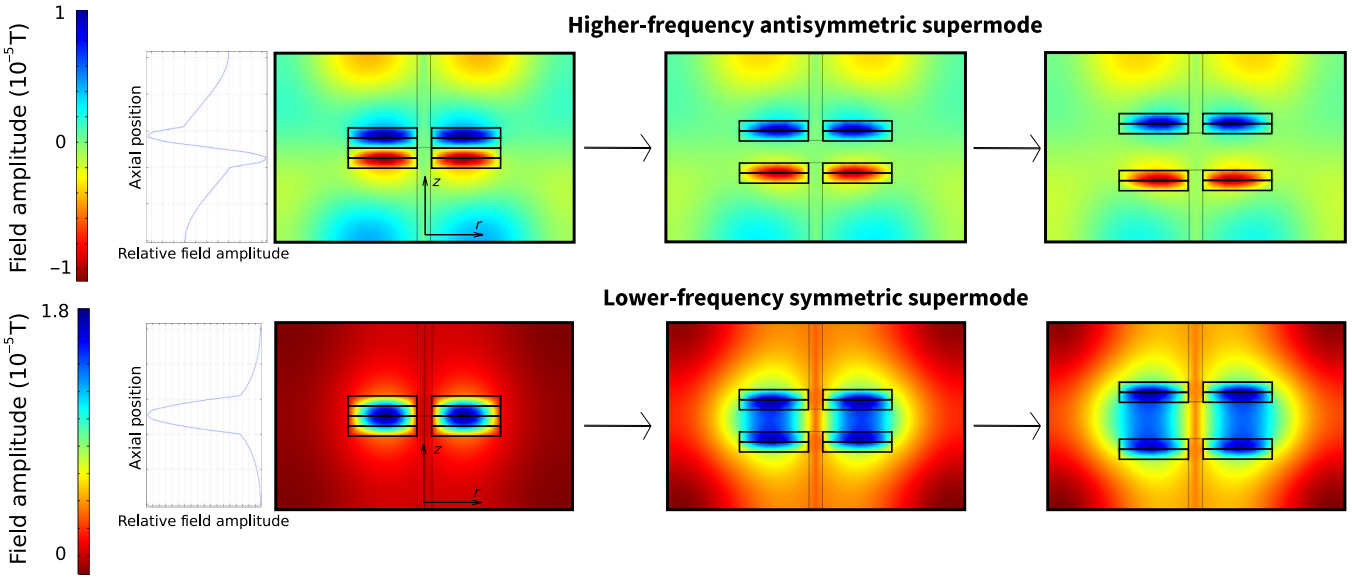

FIG. 1. B_ϕ field distribution for an antisymmetric and symmetric supermode pair. The plots on the left show B_ϕ as a function of z for fixed radius, while the axes show negative and positive field values (in T). Both representations are computed in COMSOL. As the gap is increased, the lower mode (TM_{012}-like) can be identified as having in-phase lobes in the two dielectric pieces (symmetric supermode), while the upper mode (TM_{013}-like) has similar lobes, which are out of phase (antisymmetric). In the limit where the gap spacing is large, the frequency of the symmetric mode approaches the frequency of the antisymmetric mode, depending on the mode confinement within the dielectric. The symmetric supermode is sensitive to axions, as the field is largely in phase across the volume, while the antisymmetric mode is not. The sapphire disks are represented by heavy dark lines.

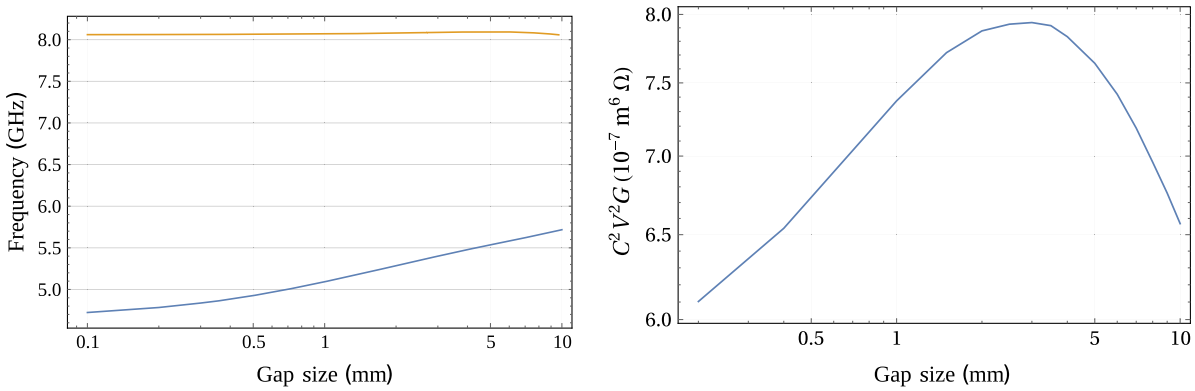

FIG. 2. Calculated frequencies (in GHz) for the symmetric and antisymmetric supermodes (left panel, blue and orange lines, respectively), and the C^2V^2G product for the symmetric supermode (right panel) vs gap size (in mm) for the disk resonator discussed in the text.

fixed value of r presented in Fig. 1, we can see that the symmetric mode conforms to this field structure for a p value of 2, with some compression and distortion due to the presence of the dielectric, while the antisymmetric mode conforms to a p value of 3, with similar compression and distortion. This supermode interaction can provide large-frequency tuning ranges over small displacements. In an ideal situation, the uppermost disk would be displaced upwards, while the lower disk would be displaced downwards to maintain symmetry. In practice, it is more feasible to leave one disk stationary and adjust the position of the other relative to it. Over a short tuning range, this is not a large deviation from the ideal. For the specific parameters which are modeled for our study, in order to achieve tuning of roughly 500 MHz from the starting frequency of 4.66 GHz, it is necessary to increase the gap between the disks by only a small fraction (2%) of the length of the resonator (in this case, 1 mm). The C^2V^2G product and resonant frequencies as a function of gap size for this example (cavity radius of approximately 41 mm, height of about 50 mm, sapphire radius of 21 mm, sapphire height of 2.74 mm, central teflon post radius of 2 mm, and a symmetric supermode starting frequency of 4.66 GHz) are shown in Fig. 2. These dimensions are chosen due to the availability of materials, but the resonator may be arbitrarily scaled to provide any desired frequency.

We perform proof-of-concept measurements to verify that the modes behave as expected. A resonator with the above dimensions is constructed, and the disks are placed on teflon rods. The lower disk remains stationary, while the upper disk is displaced upwards using a micrometer, which of course yields slightly different results than those presented in Fig. 2. Two probes are inserted into the cavity to read out the relevant modes in transmission. The expected and measured frequencies as a function of gap size are presented in Fig. 3.

This resonant structure is valuable as it contains a built-in highly responsive frequency-tuning mechanism and is readily scalable to different frequencies. Furthermore, it is a relatively simple structure compared to other proposed resonators that rely on many more dielectric disks or slabs, and it is more practical to implement experimentally. The responsiveness of the resonant frequency to position displacement is particularly appealing, combined with the fact that spurious mode density in the region is very low.

We decide to investigate the effect of tuning multiple disks (where n equals the number of disks) in our cavity resonator by implementing a finite-element model in COMSOL. The results are shown in Fig. 4. In this case, we implement a copper cavity of radius 31 mm and height

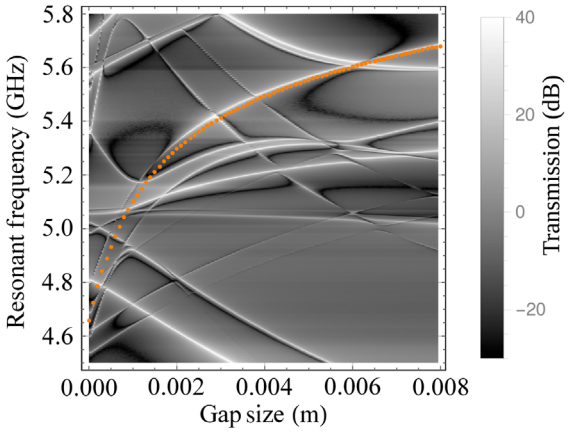

FIG. 3. Density plot of transmission measurements in the proof-of-concept experiment. Lighter colors represent more transmission, whereas darker colors represent less transmission. The orange overlaid data represents the frequency of the most sensitive mode vs gap size computed via finite-element analysis. We attribute the frequency discrepancy at small gap sizes to a misalignment between the two disks, which has less impact on the modes as the gap size increases. We observe multiple mode crossing with dissimilar modes, while the higher-frequency antisymmetric supermode is too high in frequency (roughly 8 GHz, per Fig. 2) to be observed in this plot.

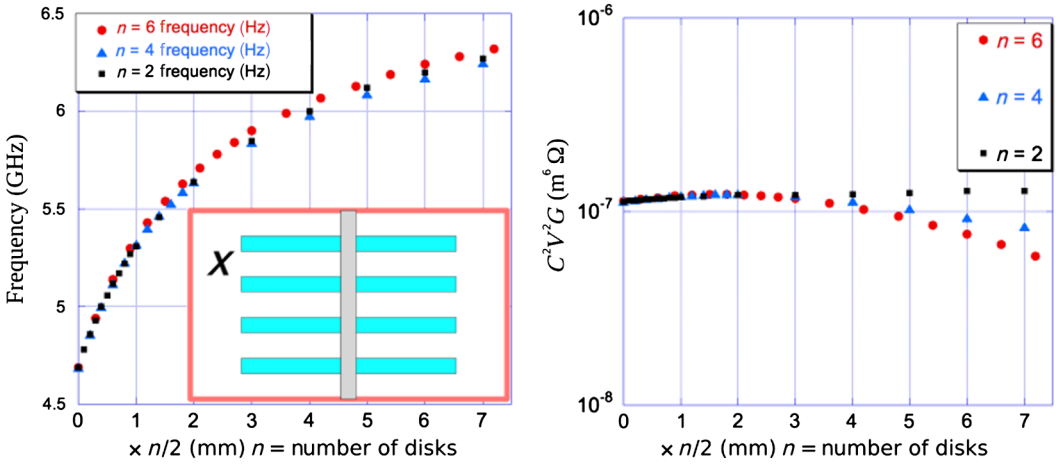

FIG. 4. Comparison of supermode frequency tuning (left panel) and sensitivity (right panel) as a function of $x \times n/2$. The inset in the left panel shows a schematic of a multidisk resonator of $n = 4$, with each disk separated by x mm.

37 mm, with multiple disks supported by a central sapphire rod 3 mm in diameter. Here, we assume that the amount of sapphire remains constant in each simulation, i.e., for $n = 2$, the individual disk's height is 6 mm, for $n = 4$, the individual disk's height is 3 mm, and for $n = 6$, the individual disk's height is 2 mm. The equivalent supermode behaves in a very similar way in all cases, as can be seen in Fig. 4, where we show the frequency and the C^2V^2G value versus $x \times n/2$, where x is the individual gap between two adjacent disks. Thus, for simplicity (and for sensitivity) the $n = 2$ choice is optimum for this type of tuning. Introducing more disks will lead to greater technical difficulties in simultaneously tuning all disks, and it does not yield an increased sensitivity. Higher-order modes equivalent to those used by Electric Tiger and MADMAX will exist; however, in a closed cavity, the density of modes would be too great: these types of modes are best suited to open resonators to avoid mode crowding. To keep the high Q factor of the supermodes, the cavity must be present, as the relevant modes are of low azimuthal order, and the modes would thus radiate a significant amount of energy without a cavity and exhibit a degraded Q factor.

B. Dielectric rings

The previous supermode scheme based on disks has a reduced form factor and volume due to much of the in-phase field being present in the dielectric [see Eq. (1)]. To improve on this and confine most of the energy in a larger volume and in free space, we propose another supermode scheme that relies on hollow dielectric cylinders of carefully selected thickness and located correctly within a cylindrical conducting shell. This setup is similar to a Bragg resonator but requires different conditions to achieve optimal axion sensitivity, so we name the resonators "dielectric boosted axion sensitivity" (DBAS) resonators.

In a traditional Bragg resonator, a dielectric layer inside a cavity creates a virtual boundary condition and thus increases the geometry factor of the resonance, as the mode electromagnetic field is shielded from the comparatively lossy conducting cavity walls. This effect is well documented in the literature for a variety of nonaxion-sensitive transverse-electric modes, and it is used to boost quality factors, as all wall losses may be decoupled from the mode simultaneously [36–40]. For this effect to work, the electric-field pattern of the mode must be tangential to the cavity walls. Thus, to apply it to an axion-sensitive TM mode only the cylindrical walls can make use of the Bragg effect. This effect may be achieved by increasing the radius of the cavity slightly and placing a dielectric boundary inside.

When the correct parameters, such as the dielectric thickness and the size of the gap between the dielectric and the conducting walls are met, the geometry factor of the resonance increases dramatically, the frequency decreases slightly, and the axion form factor decreases due to the increase in overall volume. A representation of the z-direction electric field of a TM_{020} mode (again computed via finite-element analysis), confined by a sapphire cylinder such that the Bragg condition is met, is shown in Fig. 5. The geometry factor in this case is increased by a factor of approximately 1.4 when compared with an empty TM_{020} resonator at the same frequency. This effect may be applied to any mode in the TM_{0n0} family; however, the location and dimensions of the ring relative to the outer wall of the cavity for the optimal geometry factor will be different for each mode.

1. Bragg resonators for TM modes

We investigate this effect for different TM modes via finite-element modeling in COMSOL MULTIPHYSICS and perform proof-of-concept measurements. For fixed sapphire ring dimensions (outer radius of 24.41 mm and thickness of 3.4 mm) we vary the size of the gap between the walls of the resonator and the interior sapphire ring, computing the geometry factors and frequencies of the first four TM modes. The results of this finite-element modeling, with overlayed experimental results and including measured quality factors, are shown in Fig. 6 and

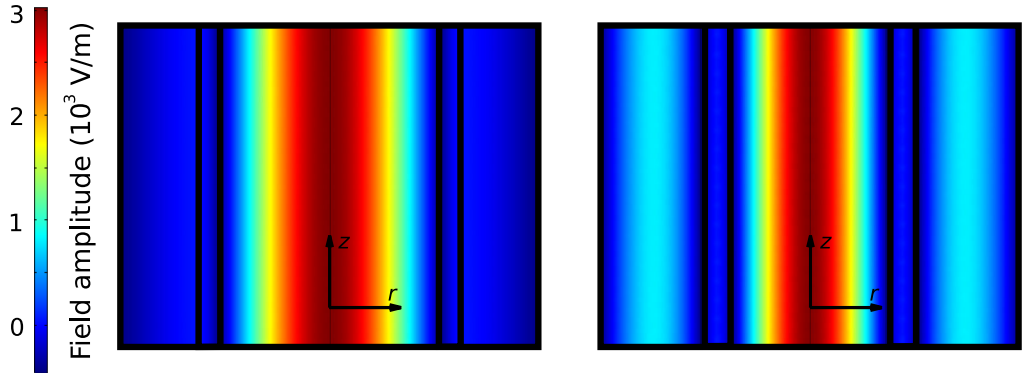

FIG. 5. A 2D axisymmetric visualization of the z component of the electric field for a TM_{020}-like mode confined inside a sapphire ring, such that the Bragg effect is achieved (left panel), and a similar visualization of a TM_{030}-like mode designed such that the out-of-phase electric field is contained in the sapphire ring and suppressed. We name this phenomenon the dielectric boosted axion sensitivity (DBAS) effect (right panel). The sapphire rings are represented by heavy dark lines.

Table I. While such resonators boast increased quality factors compared to traditional TM modes, they are not the most axion-sensitive resonant structures that can be constructed with dielectric rings.

2. Dielectric boosted axion sensitivity, or DBAS, resonators

As discussed previously, it is possible to use dielectrics to alter the axion coupling to a cavity resonance by changing the field structure within the cavity. Consider that, for a TM_{0n0} mode inside a cylindrical resonator,

$$\vec{E}_c(r) = E_0 e^{i\omega t} J_0\left(\frac{\zeta_{0,n}}{R} r\right)\hat{z}, \qquad R = \frac{\zeta_{0,n} c}{\omega},$$

where $\vec{E}_c$ is the mode electric field, E_0 is a constant related to the amplitude of the field, ω is the mode angular resonant frequency, J_0 is the zeroth-order Bessel J function, $\zeta_{0,n}$ is the nth root of the zeroth-order Bessel J function, R is the cavity radius, r is the radial distance from the center of the cavity, $\hat{z}$ is the cavity z-direction unit vector, and c is the speed of light. The z component of the electric field takes the form of a Bessel J function and alternates in phase accordingly, as illustrated for a TM_{030} mode in Fig. 7.

Upon inspection of Eq. (1), it is clear that the form factor would increase if a higher proportion of the z component of the electric field is in the same phase, as the numerator of the first term in the expression would increase. In order to achieve this increase, we can place a dielectric ring with the correct thickness and in the correct position such that the out-of-phase electric field is confined in the dielectric, and thus its contribution to the form factor is reduced. This technique will not work for a TM_{010} mode, where the field is all in the same direction, and tends to work best for odd-numbered modes.

To illustrate this effect, we shall consider a TM_{030} mode. We know that the radial distance from the center of the

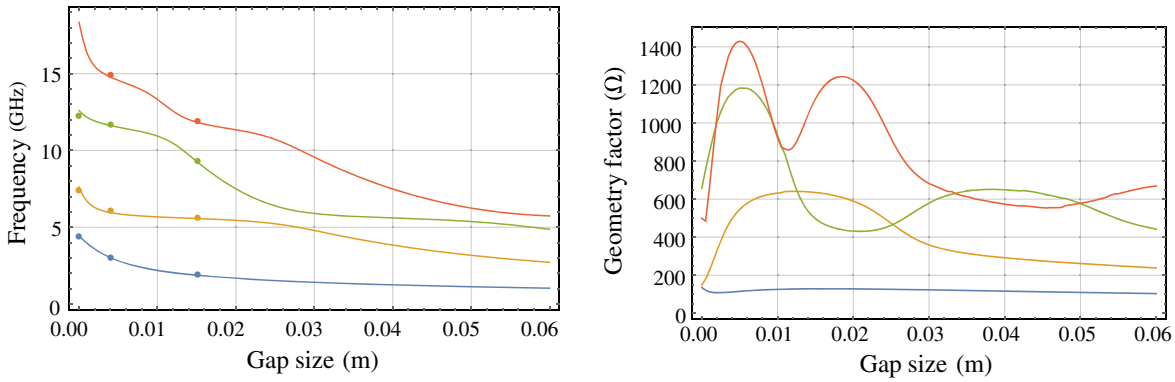

FIG. 6. Resonant frequencies (left panel) and geometry factors (right panel) as a function of the size of the gap between the sapphire ring and the cavity wall, computed via finite-element analysis for the first four TM modes. TM_{010} is shown in blue, TM_{020} in orange, TM_{030} in green, and TM_{040} in red. The sapphire ring is of fixed dimensions (outer radius of 24.41 mm, thickness of 3.24 mm, and height of 31.98 mm). The TM modes become Bragg confined modes in the regions where the geometric factor is enhanced and the field is antiresonant in the reflectors. These regions can be seen to be quite broad over gap-size variations. Experimental measurements of mode frequencies from cryogenic proof-of-concept measurements are overlaid on the left plot.

TABLE I. Measured quality factors for the first four TM modes from proof-of-concept experiments.

Mode	Quality factor (sapphire ring)	Frequency (sapphire ring) (GHz)
TM_{010}	25 028	1.92
TM_{020}	75 086	5.63
TM_{030}	98 600	11.694
TM_{040}	63 120	14.96

resonator to the point where the field changes direction is given by

$$r = \frac{\zeta_{0,1}}{\zeta_{0,3}} R \sim 0.278R. \tag{4}$$

We should leave this region as vacuum, as we do not wish to reduce the contribution of this section of the field to the form factor. We also know that the radial distance from the center to the point where the field changes direction for the second time, i.e., comes back into phase with the first region, is given by

$$r = \frac{\zeta_{0,2}}{\zeta_{0,3}} R.$$

Thus, we conclude that the region containing an electric field out of phase with the other two regions is of width

$$\frac{\zeta_{0,2} - \zeta_{0,1}}{\zeta_{0,3}} R \sim 0.36R, \tag{5}$$

beginning at $r = [(\zeta_{0,1})/(\zeta_{0,3})]R$. The final vacuum region of in-phase field is of thickness

$$\frac{\zeta_{0,3} - \zeta_{0,2}}{\zeta_{0,3}} R \sim 0.362R. \tag{6}$$

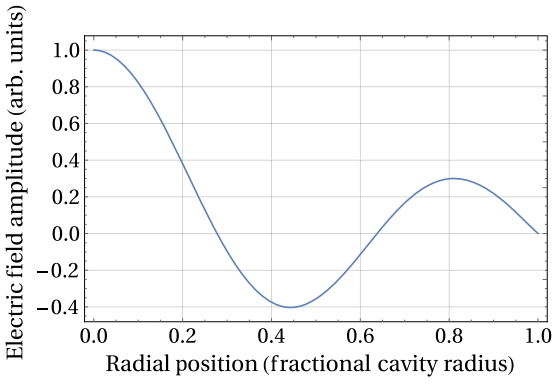

FIG. 7. Representation of the E_z component of the TM_{030} mode as a function of radial distance from the center of the cavity. The mode takes the form of a Bessel J function.

The middle, out-of-phase region in Eq. (5) is the region in which we wish to place a dielectric. Considering that the speed of light is reduced in a dielectric medium by a factor of $\sqrt{\epsilon_r}$, we can consider the space inside the dielectric to be effectively increased by this same factor. Thus, to meet our condition that the out-of-phase field be confined in the medium, we construct our dielectric region such that its size is reduced compared with Eq. (5) by the same factor.

Put simply, our dielectric ring should have the thickness

$$\frac{\zeta_{0,2} - \zeta_{0,1}}{\zeta_{0,3}\sqrt{\epsilon_r}} R \sim 0.107R \tag{7}$$

for sapphire, $\epsilon_r \sim 11.349$. Now, of course, as the middle region is reduced in size by a factor of $\sqrt{\epsilon_r}$, which is over 3 for sapphire, these fractions of R [0.278, 0.107, and 0.362; Eqs. (4), (6), and (7)] do not sum to unity but are, rather, fractions *relative* to one another. That is to say, the ratio of the first vacuum region thickness to the sapphire region thickness should be $\frac{0.278}{0.107}$. In order to simplify this process, we can multiply all of the relevant thicknesses by $\frac{1}{0.278+0.107+0.362} \sim 1.34$ such that they sum to unity. Specifically, the regions should be of thicknesses $0.372R$, $0.143R$, and $0.485R$, respectively.

As an aside, this increase in size makes intuitive sense, as the introduction of the dielectric reduces the frequency of the cavity slightly, and the ratio by which we multiply the values is almost exactly equal to the ratio of the radius of an equivalent-frequency empty cavity to the radius of the cavity containing the dielectric ring. We may equivalently think of it as follows: the regions should be of the thicknesses presented in Eqs. (4), (6), and (7) if we replace R in these equations by R', the radius of a larger cavity increased in size relative to the cavity containing the dielectric ring by a factor of approximately 1.34 (for sapphire), such that the frequency of this larger empty cavity is the same as that of the smaller cavity containing the ring. Consider R' the *effective* radius of the cavity due to the effect of the dielectric.

While hopefully illustrative, this method is not very helpful in designing a cavity, as we do not know what the final frequency of the ring cavity is going to be until we have decide on a ring thickness, which, by this method, we cannot find until we know the radius R' of the larger equivalent cavity—which we, in turn, cannot find until we know the final ring-cavity frequency. We should instead opt for the "sum-to-unity" method outlined above and employ thicknesses of $0.372R$, $0.143R$, and $0.485R$ for the first-vacuum, dielectric, and second-vacuum regions, respectively (for sapphire, in a TM_{030} mode, this same process may be followed for other materials in other modes). These are the dimensions for the air and sapphire layers that should be chosen if we wish only to constrain the out-of-phase field within the dielectric and maximize our axion cavity form factor. This method can be easily extended

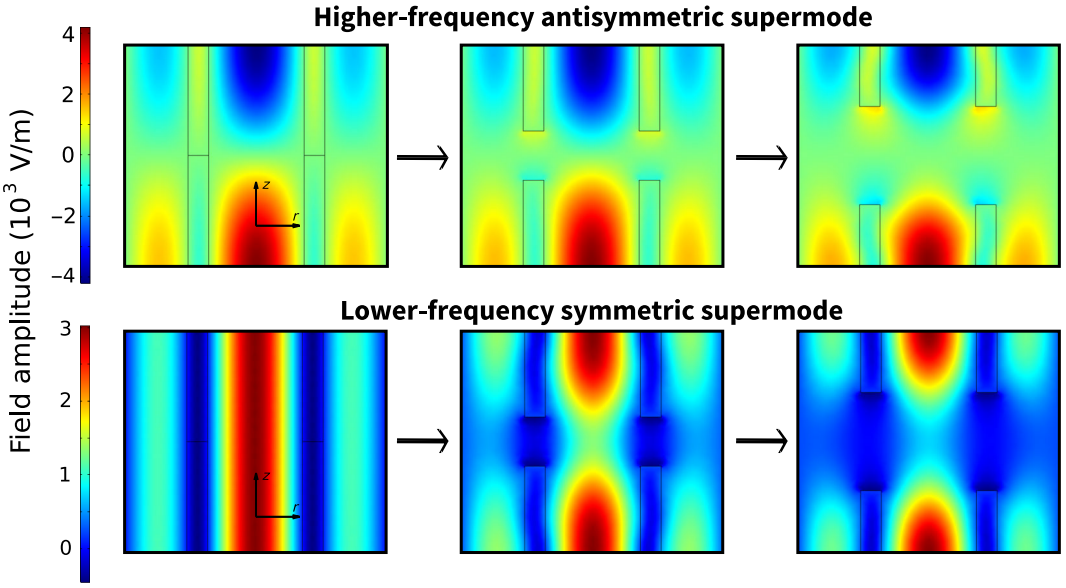

FIG. 8. E_z field distribution for the two modes discussed in the text as the gap between the sapphire rings increases. Redder colors represent higher positive E_z values, whereas bluer colors represent higher negative field values. The lower mode is a TM_{030}-like mode, with high axion sensitivity, whereas the higher mode is a TM_{031}-like mode with no axion sensitivity.

following the above methodology to any odd n-valued TM_{0n0} mode, with $(n-1)/2$ layers of dielectric. The TM_{030} mode is presented here, as it is the most straightforward and most experimentally practical to implement, requiring only one dielectric ring.

We conduct finite-element modeling of a TM_{030}-like resonator with a sapphire ring placed to satisfy the conditions above, and we can report form factors on the order of 0.47, compared to 0.053 for an empty-cavity TM_{030} mode. Furthermore, the geometry factor with the correctly placed sapphire is 791, compared to 269 for an empty TM_{010} cavity of the same frequency and aspect ratio. A representation of the z-direction electric field in this case is shown in Fig. 8.

Interestingly, we can exploit a supermode-type tuning effect with this structure in a similar fashion to the disk structure discussed above. If we split the dielectric ring in the axial direction, we observe that there are again two modes, the symmetric TM_{030} mode occupying the entire dielectric ring, and a higher-frequency antisymmetric mode which contains a single variation in the longitudinal direction, a TM_{031} mode. If we increase the gap size between the two parts of the ring, we observe that the frequency of the axion-sensitive symmetric supermode, TM_{030}, increases while retaining good sensitivity. For a cavity with a radius of 63.8 mm and a height of 108 mm, and a sapphire ring of thickness 9.12 mm with a TM_{030}-like starting frequency 4.83 GHz, we observe tuning of approximately 1.6 GHz as the ring is separated and removed from the cavity. The C^2V^2G product and resonant frequencies for this resonator, computed via finite-element analysis is shown in Fig. 9. This supermode tuning scheme works the same way for either a traditional Bragg resonator or the DBAS resonator. We stress that this or similar techniques could be applied to other Bragg resonant structures, in other applications, to create highly tunable resonators. For example, the same ideas could be applied to high-Q TE modes based on Bragg reflectors to create highly tunable cavities, whereas traditional Bragg resonators are stationary in frequency.

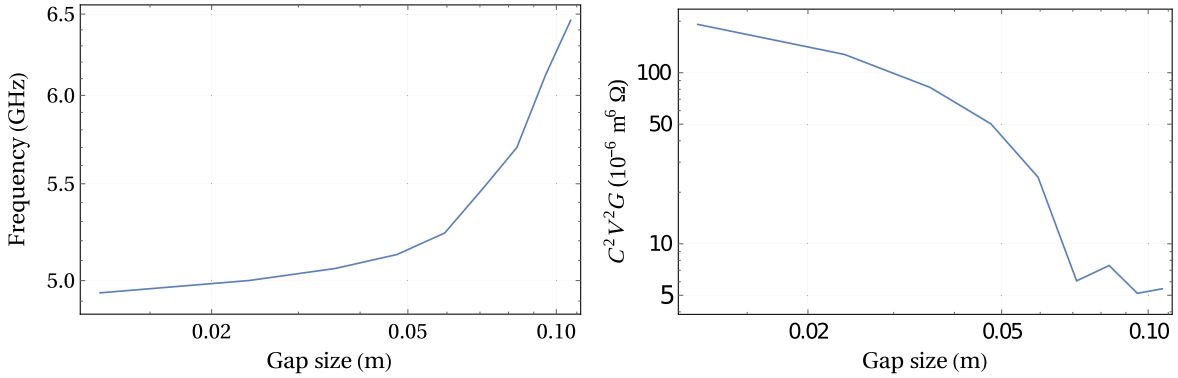

FIG. 9. (Left panel) Frequency (in GHz), and (right panel) C^2V^2G product vs gap size (in m) for the ideal DBAS resonator discussed in the text.

These dimensions are chosen so that the resonator could be compared to the sapphire disk resonator. It is important to note that, similar to tuning the sapphire disk resonator, there are practical considerations in the design of a DBAS-effect resonator. In order to reduce complexity, we may again choose to displace only one of the two rings inside the cavity, adjusting the gap between them. In such a case, it is optimal to place the break in the ring below the halfway point, as this positioning provides more symmetry over the range of tuning. With the break in the middle, the only point of axial symmetry is at zero gap, whereas, with the cut below the middle, there are two points of axial symmetry over the tuning range.

It is worth noting that, while there are mode crossings with azimuthally varying ($m > 0$) modes, a finite-element analysis does not predict avoided level crossings and an associated reduction in sensitivity. We believe that this lack of predicted avoided level crossings is a result of orthogonality between these higher-order modes and the axion-sensitive $m = 0$ mode. Consequently, it is possible to employ the standard technique of filling the resonator with a different material, such as liquid helium, and rescanning over the regions where the sensitive $m = 0$ mode crosses these higher-order modes [15].

Resonators of this type are very useful in the push towards higher-frequency haloscopes, where it is beneficial to utilize higher-order modes so that larger cavities may be employed. Traditionally, this approach has not been appealing, as the form factors for these higher-order modes are significantly reduced such that the product CV remains nearly constant. We present a scheme for utilizing large resonators with higher-order modes, while still maintaining appreciable form factors and high axion sensitivity. The scheme also comes with a built-in tuning mechanism which is highly responsive to position displacement based on supermode tuning.

It is important to note that the optimal condition for a geometry factor (the Bragg effect) and the optimal condition for a form factor (the DBAS effect) are not the same, and a trade-off may consequently be required. The optimal C^2V^2G product may occur for a slightly different dielectric thickness and location depending on the specific parameters of the cavity and experiment, such as length, mode frequency, and desired tuning range. In order for a shift away from the DBAS condition to be optimal, we must be gaining in geometry factor much faster than we are losing in form factor (as the figure of merit depends on the form factor quadratically, but only linearly in geometry factor), but this condition may be possible depending on the specific geometry of the resonator under design, and the relative narrowness or broadness of the Bragg and DBAS regions. This scenario is very complex to model analytically, so, in order to design resonators for a haloscope based on these techniques, we employ an iterative method where we adjust the dielectric thickness and location (starting with the DBAS result and making small changes) and compare results until the optimal parameters are found. An example of results of this kind of iterative process are shown in Fig. 10. In any case, we may wish to call the optimal resonator (which may be a hybrid Bragg and DBAS resonator) a "Bragg-Axion" or "Braxion" resonator.

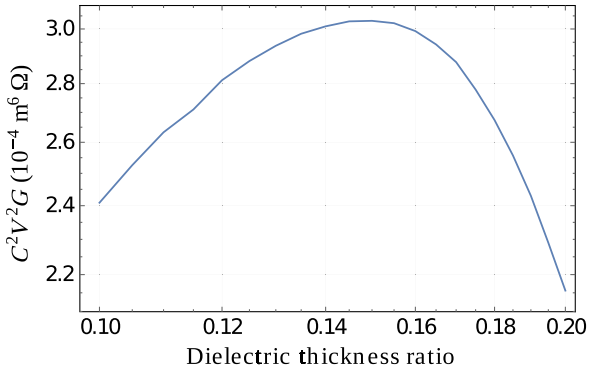

FIG. 10. C^2V^2G product versus thickness of the dielectric region as a fraction of cavity radius, with each point scaled to 5 GHz for comparison. The gap size and other parameters are kept constant in this sweep. As shown, the optimum lies near 0.15, which is close to what is predicted in the text for the DBAS effect.

C. Comparison with a traditional tuning rod

It is a common technique for tuning a haloscope to introduce a conducting rod into the cavity, and slide it radially from the outer region of the cavity into the center. This conducting rod breaks symmetry in the TM_{0n0} mode family and alters the frequency of the cavity. We present a C^2V^2G plot and the tuning range for such a cavity (Fig. 11), employing a TM_{010} mode, computed via finite-element analysis. This cavity is designed such that the tuning range and frequencies are comparable to the two schemes presented in this article. It is clear from the results that the DBAS resonator scheme proposed here outperforms the traditional tuning rod in a TM_{010} cavity around 5 GHz. The DBAS resonator has C^2V^2G products that are, at their peak, between 1 and 2 orders of magnitude greater than the traditional tuning rod. The dielectric disk scheme has C^2V^2G products that are lower by an order of magnitude; however, the resonator tunes extraordinarily quickly, and spurious mode density in the neighborhood is low. This type of resonator would be of interest in an experiment that requires a very fast scanning rate, such as those proposed to search for streaming dark matter [41]. We consider these, particularly the DBAS resonator, to be valuable resonant structures for axion haloscopes, and such resonators will be employed in the forthcoming ORGAN experiment [42].

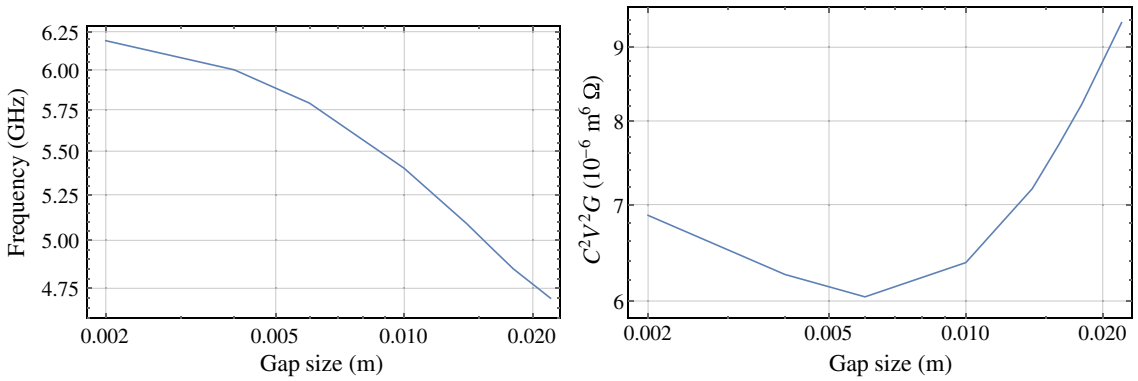

FIG. 11. (Left panel) Frequency (in GHz), and (right panel) C^2V^2G product vs rod distance from the center of the cavity (in m) for the conducting rod-tuned resonator discussed in the text.

IV. CONCLUSION

In this article, we present two interesting dielectric resonator designs for axion haloscopes. Additionally, the concept of a Bragg resonator is applied to TM modes showing increased quality factors, rather than the usual TE modes for such structures. Both haloscope schemes have built-in tuning mechanisms that are highly responsive to position displacement based on supermode interactions. The first haloscope scheme confines most of the field in the dielectric, while the second confines only the lesser, out-of-phase field components in the dielectric. The advantages of these schemes in regard to different axion searches are discussed. The microwave cavity Bragg and dielectric boosted axion sensitivity conditions are discussed and compared, as they are different. Results of the finite-element analysis allow the optimization of the sensitivity and scan rate based on the figure of merit, C^2V^2G. We undertake a proof-of-concept experiment for the dielectric disk resonator scheme, as well as for the Bragg effect in TM modes, showing good agreement with the modeling. Finally, we compare these two resonator schemes with a traditional conducting rod-tuned haloscope and find that particularly the second proposed scheme, the DBAS resonator, is far superior.

ACKNOWLEDGMENTS

This work was funded by Australian Research Council (ARC) Grant No. CE170100009, the Australian Government's Research Training Program, and the Bruce and Betty Green Foundation.

[1] Joerg Jaeckel and Andreas Ringwald, The low-energy frontier of particle physics, Annu. Rev. Nucl. Part. Sci. **60**, 405 (2010).
[2] R. D. Peccei and Helen R. Quinn, *CP* Conservation in the Presence of Pseudoparticles, Phys. Rev. Lett. **38**, 1440 (1977).
[3] J. Ipser and P. Sikivie, Can Galactic Halos Be Made of Axions?, Phys. Rev. Lett. **50**, 925 (1983).
[4] P. Sikivie, Experimental Tests of the "Invisible" Axion, Phys. Rev. Lett. **51**, 1415 (1983).
[5] P. Sikivie, Detection rates for "invisible"-axion searches, Phys. Rev. D **32**, 2988 (1985).
[6] S. J. Asztalos, G. Carosi, C. Hagmann, D. Kinion, K. van Bibber, M. Hotz, L. J. Rosenberg, G. Rybka, J. Hoskins, J. Hwang, P. Sikivie, D. B. Tanner, R. Bradley, and J. Clarke, Squid-Based Microwave Cavity Search for Dark-Matter Axions, Phys. Rev. Lett. **104**, 041301 (2010).
[7] J. Hoskins, J. Hwang, C. Martin, P. Sikivie, N. S. Sullivan, D. B. Tanner, M. Hotz, L. J. Rosenberg, G. Rybka, A. Wagner, S. J. Asztalos, G. Carosi, C. Hagmann, D. Kinion, K. van Bibber, R. Bradley, and J. Clarke, Search for nonvirialized axionic dark matter, Phys. Rev. D **84**, 121302 (2011).
[8] L. F. Abbott and P. Sikivie, A cosmological bound on the invisible axion, Phys. Lett. **120B**, 133 (1983).
[9] John Preskill, Mark B. Wise, and Frank Wilczek, Cosmology of the invisible axion, Phys. Lett. **120B**, 127 (1983).
[10] Jihn E. Kim, Weak-Interaction Singlet and Strong *CP* Invariance, Phys. Rev. Lett. **43**, 103 (1979).
[11] Jihn E. Kim and Gianpaolo Carosi, Axions and the strong *CP* problem, Rev. Mod. Phys. **82**, 557 (2010).
[12] Michael Dine, Willy Fischler, and Mark Srednicki, A simple solution to the strong *CP* problem with a harmless axion, Phys. Lett. **104B**, 199 (1981).
[13] M. A. Shifman, A. I. Vainshtein, and V. I. Zakharov, Can confinement ensure natural *CP* invariance of strong interactions?, Nucl. Phys. **B166**, 493 (1980).
[14] Michael Dine and Willy Fischler, The not-so-harmless axion, Phys. Lett. **120B**, 137 (1983).
[15] Edward John Daw, Ph.D. thesis, Massachusetts Institute of Technology, 1998.
[16] Ben T. McAllister, Stephen R. Parker, and Michael E. Tobar, Axion Dark Matter Coupling to Resonant Photons via Magnetic Field, Phys. Rev. Lett. **116**, 161804 (2016); **117**, 159901(E) (2016).
[17] I. Stern, A. A. Chisholm, J. Hoskins, P. Sikivie, N. S. Sullivan, D. B. Tanner, G. Carosi, and K. van Bibber, Cavity design for high-frequency axion dark matter detectors, Rev. Sci. Instrum. **86**, 123305 (2015).

[18] Jerzy Krupka, Krzysztof Derzakowski, Michael Tobar, John Hartnett, and Richard G. Geyer, Complex permittivity of some ultralow loss dielectric crystals at cryogenic temperatures, Meas. Sci. Technol. **10**, 387 (1999).

[19] J. Krupka, K. Derzakowski, A. Abramowicz, M. E. Tobar, and R. G. Geyer, Use of whispering-gallery modes for complex permittivity determinations of ultra-low-loss dielectric materials, IEEE Trans. Microwave Theory Tech. **47**, 752 (1999).

[20] Michael Edmund Tobar, Jerzy Krupka, Eugene Nicolay Ivanov, and Richard Alex Woode, Anisotropic complex permittivity measurements of mono-crystalline rutile between 10 and 300 K, J. Appl. Phys. **83**, 1604 (1998).

[21] Gray Rybka, Andrew Wagner, Aryeh Brill, Katleiah Ramos, Robert Percival, and Kunal Patel, Search for dark matter axions with the Orpheus experiment, Phys. Rev. D **91**, 011701(R) (2015).

[22] Allen Caldwell, Gia Dvali, Béla Majorovits, Alexander Millar, Georg Raffelt, Javier Redondo, Olaf Reimann, Frank Simon, and Frank Steffen (MADMAX Working Group), Dielectric Haloscopes: A New Way to Detect Axion Dark Matter, Phys. Rev. Lett. **118**, 091801 (2017).

[23] T. M. Shokair, J. Root, K. A. Van Bibber, B. Brubaker, Y. V. Gurevich, S. B. Cahn, S. K. Lamoreaux, M. A. Anil, K. W. Lehnert, B. K. Mitchell, A. Reed, and G. Carosi, Future directions in the microwave cavity search for dark matter axions, Int. J. Mod. Phys. A **29**, 1443004 (2014).

[24] Ben T. McAllister, Stephen R. Parker, and Michael E. Tobar, 3D lumped *LC* resonators as low mass axion haloscopes, Phys. Rev. D **94**, 042001 (2016).

[25] P. Sikivie, N. Sullivan, and D. B. Tanner, Proposal for Axion Dark Matter Detection Using an *LC* Circuit, Phys. Rev. Lett. **112**, 131301 (2014).

[26] Yonatan Kahn, Benjamin R. Safdi, and Jesse Thaler, Broadband and Resonant Approaches to Axion Dark Matter Detection, Phys. Rev. Lett. **117**, 141801 (2016).

[27] Woohyun Chung, CULTASK, the coldest axion experiment at CAPP/IBS in Korea, *Proc. Sci.*, CORFU2015 (2016) 047.

[28] B. M. Brubaker *et al.*, First Results from a Microwave Cavity Axion Search at 24 μeV, Phys. Rev. Lett. **118**, 061302 (2017).

[29] Ben T. McAllister, Stephen R. Parker, Eugene N. Ivanov, and Michael E. Tobar, in *Proceedings of the 12th Patras Workshop on Axions, WIMPs and WISPs (PATRAS 2016), Jeju Island, South Korea, 2016*, edited by Y. Kim, A. Lindner, and Y. K. Semertzidis (Verlag Deutsches Elektronen-Synchrotron, Hamburg, 2016), pp. 116–120.

[30] Guillermo Ballesteros, Javier Redondo, Andreas Ringwald, and Carlos Tamarit, Unifying Inflation with the Axion, Dark Matter, Baryogenesis and the Seesaw Mechanism, Phys. Rev. Lett. **118**, 071802 (2017).

[31] Benjamin Phillips, in Proceedings of the 2nd Workshop on Microwave Cavities and Detectors for Axion Research, Livermore, CA, 2017 (unpublished).

[32] James Sloan, in Proceedings of the 1st Workshop on Microwave Cavity Design for Axion Detection, Livermore, CA, 2015 (unpublished).

[33] Qiang Lin, Jessie Rosenberg, Darrick Chang, Ryan Camacho, Matt Eichenfield, Kerry J. Vahala, and Oskar Painter, Coherent mixing of mechanical excitations in nano-optomechanical structures, Nat. Photonics **4**, 236 (2010).

[34] Ivan S. Grudinin, Hansuek Lee, O. Painter, and Kerry J. Vahala, Phonon Laser Action in a Tunable Two-Level System, Phys. Rev. Lett. **104**, 083901 (2010).

[35] B. D. Cuthbertson, M. E. Tobar, E. N. Ivanov, and D. G. Blair, Parametric backaction effects in a high-Q cyrogenic sapphire transducer, Rev. Sci. Instrum. **67**, 2435 (1996).

[36] Jean-Michel le Floch, Michael E. Tobar, David Mouneyrac, Dominique Cros, and Jerzy Krupka, Discovery of Bragg confined hybrid modes with high Q factor in a hollow dielectric resonator, Appl. Phys. Lett. **91**, 142907 (2007).

[37] Jean-Michel le Floch, Michael E. Tobar, Dominique Cros, and Jerzy Krupka, Low-loss materials for high Q factor Bragg reflector resonators, Appl. Phys. Lett. **92**, 032901 (2008).

[38] M. E. Tobar, D. Cros, P. Blondy, and E. N. Ivanov, Compact, high-Q, zero temperature coefficient, TE_{011} sapphire-rutile microwave distributed bragg reflector resonators, IEEE Trans. Ultrason. Ferroelectr. Freq. Control **48**, 821 (2001).

[39] M. E. Tobar, J. M. Le Floch, D. Cros, J. Krupka, J. D. Anstie, and J. G. Hartnett, Spherical Bragg reflector resonators, IEEE Trans. Ultrason. Ferroelectr. Freq. Control **51**, 1054 (2004).

[40] J. Krupka, A. Cwikla, M. Mrozowski, R. N. Clarke, and M. E. Tobar, High Q-factor microwave Fabry-Perot resonator with distributed Bragg reflectors, IEEE Trans. Ultrason. Ferroelectr. Freq. Control **52**, 1443 (2005).

[41] K. Zioutas *et al.*, Search for axions in streaming dark matter, arXiv:1703.01436.

[42] Ben T. McAllister, Graeme Flower, Eugene N. Ivanov, Maxim Goryachev, Jeremy Bourhill, and Michael E. Tobar, The ORGAN experiment: An axion haloscope above 15 GHz, Phys. Dark Universe **18**, 67 (2017).